Experimental and numerical validation of shallow water flow around a surcharging manhole

Georges Kesserwani[1], Seungsoo Lee[1], Matteo Rubinato[1] and James Shucksmith[1]

[1]Department of Civil Engineering and Structural Engineering, University of Sheffield, Sheffield, UK (Email: g.kesserwani@shef.ac.uk, seungsoo.lee@shef.ac.uk, m.rubinato@shef.ac.uk, j.shucksmith@shef.ac.uk)

Abstract
Numerical simulation of sewer overflow into a main free-surface flow is studied and validated with respect to experimental data. A physical model of a linked floodplain and sewer system is used to carry out measurements under steady state flow conditions, considering systematic increase in the sewer surcharge. The depth-averaged Shallow Water Equations (SWE) are employed to model floodplain flow, in which sewer overflow is accounted for as an extra source term contribution. A finite volume shock-capturing scheme is tailored to solve the SWE on a non-uniform 2D mesh according to the characteristics of physical model. Steady numerical simulations are achieved. Numerical results and experimental datasets are compared, in terms of flood maps and depth histories, around at the local outflow area. The agreement between the experimental and numerical results is acceptable overall; however, it varied depending on the intensity of sewer surcharge, and on the choice of downstream boundary conditions.

Keywords
Floodplain flow; sewer overflow; shallow water simulator; steady state experiments.

INTRODUCTION

During urban pluvial flood conditions, overland surface flow and surcharging sewer flows interact at exchange points such as manholes and gullies (Rubinato et al. 2013). This processes is essentially 3D and can be modelled by a flow solver of the Navier-Stocks equations (Mahdizadeh et al. 2011, Valero et al. 2012). Given the prohibitive runtime costs of 3D models, it is more common to simulate the process within the scope of the 2D depth-averaged shallow water equations (SWE) under the assumption of hydrostatic pressure.

The development integrated sewer-to-floodplain models has been driven by two objectives. The first is the delivery of 2D flood models that are shock-capturing based on the finite volume method (Toro and Garcia-Navarro 2007). The second is to, numerically, represent of the flow interaction between the manhole and the floodplain. Several approaches have been proposed for modelling the hydrodynamics of sewer-to-floodplain flows, considering different numerical strategies to achieve coupled modelling. Fully-integrated 1D-2D approaches have been devised, which involve separate coupling with 1D unsteady pipe flow solver (e.g. Leandro et al. 2009, Seyoum et al. 2012). Most of these models are coupled with either a simplified 2D floodplain flow solvers (based on a 2D diffusion wave approach) or using a finite difference approach, both of which fall short in capturing a shock induced by a sewer overflow. Mahdizadeh et al. (2011, 2012) tailored a shock-capturing finite volume model for sewer-to-floodplain flows. They employed partially-integrated approach in which the inflow/outflow into/from the sewer system is realized by adding suitable source terms the SWE. Such a model, although limited by the assumption of full pipe flow, is of use as it represents the worst-case scenario of a flood hazard. Borsch and Klar (2014) developed a shock-capturing finite volume model

in the context of a fully-integrated coupling. Their model integrates pipe flow based on the concept of the "Preissmann slot" to account for mixed free-surface/pressurized flows, which operates under subcritical flow. Due to the lack of experimental datasets, such models have yet to be robustly validated.

This paper presents a new experimental dataset gathered at the water laboratory of the University of Sheffield (Section 2) and employs a shock-capturing model (Section 3) to reproduce the experimental observations. Numerical and experimental results are discussed in detail (Section 4) considering issues of numerical model tailoring, and comparisons of depth maps and histories at the local zone of the impact wave generated by the surcharged flow into the floodplain.

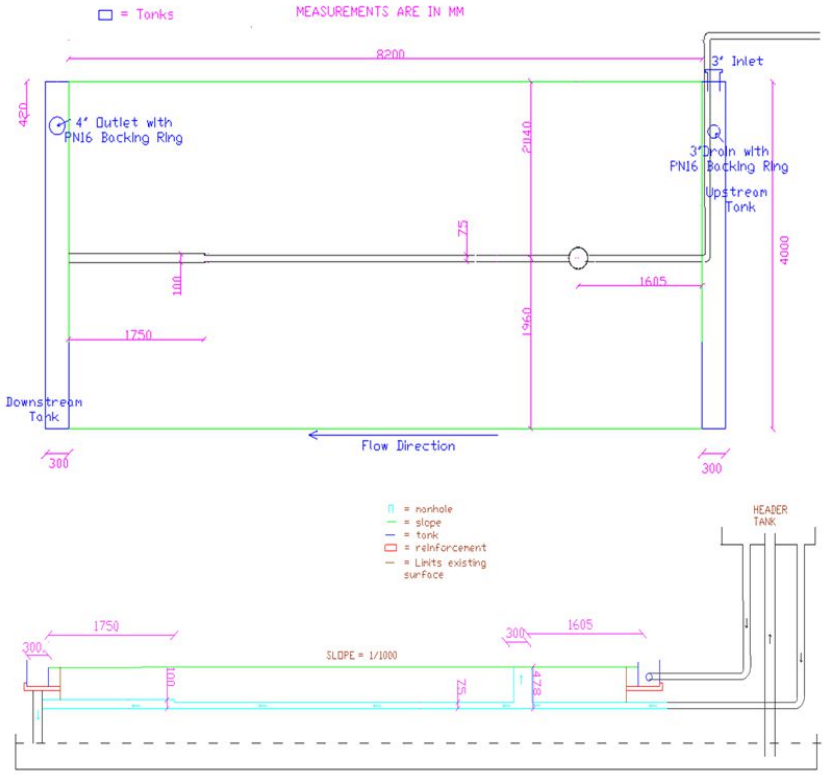

Figure 1. View from the top (upper panel) and from the side (lower panel) of the experimental apparatus

PHYSICAL MODEL

The physical model has been constructed at the hydraulic laboratory at the University of Sheffield (Rubinato, 2015). It is composed of a below-ground piped system connected to a floodplain via a scaled manhole. Flow into the pipe and the floodplain can be controlled independently via automated in line valves such that a range of floodplain (surface)/pipe (sewer) flow exchange scenarios can be reproduced. The pipe system has no slope, whereas the floodplain is inclined with a slope of 0.001. Outflow from the floodplain and pipe systems are recirculated by header tank, which feeds into the pipe and surface inlets (Figure 1).

The main pipe of the sewer system (Figure 2) has a 75mm inner diameter, and is linked to the surface flow system via a scaled manhole (diameter 240mm). The sewer system and manhole were

constructed from acrylic. Acrylic was selected for its ease of use (to retro-fit of instrumentation fixtures), transparent properties and low roughness values (Manning roughness coefficient equal to 0.01 $s/m^{1/3}$). The urban surface (Figure 2) has a length of 8.2 m, a width of 4 m and lateral the high of its lateral boundaries is 0.3 m. Inlet and outlet tanks are distributed over the full width of the system. Flow enters the inlet tank though a pipe from the laboratory header tank and flows over a shape weir crest into the surface flow system. The inlet tank is filled with a baffle material to ensure uniform flow into the system. For the test reported here, free outflow is ensured at the downstream end.

Figure 2. Below ground system consisting of a pipe connected to a manhole (left). Urban surface to which the manhole is connected (right) and the inlet tank (medium) with baffle materials.

Electro-magnetic (MAG) flow meters were installed at the upstream and downstream ends of both sewer and floodplain systems in order to measure the flow rates therein. Once the calibration of the flow meters was complete, a verification set of tests have been conducted to compare the flow rate measured by the values recorded against the values provided by the laboratory measurement tank. Based on this calibration and when applying the principles of mass conservation, the maximum anticipated measurement error in efflux discharge calculated as $Q_e = Q_1 - Q_2$ was 5.2 % (average 1.8%) and the maximum error in efflux discharge calculated $Q_e = Q_3 - Q_4$ was 4.6% (average 3.1%) over the flow ranges reported in this work (Figure 3). Around the manhole pressure sensors (GEMS series 5000) were installed to measure water levels (Figure 4). These sensors were located at points P2 and P3, located 90 mm upstream and downstream of the manhole within the main flow direction; along the *y*-direction, two sensors were symmetrically located 75 mm from the manhole (P0 and P4) and two other at a distance of 275 mm (at points P1 and P5) as shows Figure 4. Transducers were calibrated using a pointer gauge with the maximum error between measured values and defined calibration relationships quantified to be 0.72 mm.

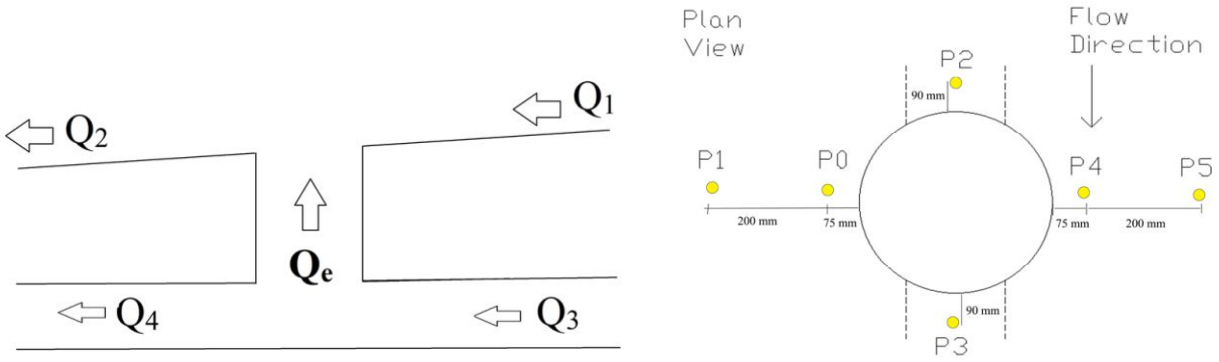

Figure 3. Inflow and outflow at the floodplain and the pipe through which the efflux Q_e can be formed (left), and sampling points P0-P5 at which water levels are recorded (right)

NUMERICAL MODEL

The depth-averaged 2D shallow water equations (SWE) are commonly used for modelling floodplain flow (Wang et al. 2011). Integrating a sewer outflow can be realized by adding suitable source terms (Mahdizadeh et al. 2011). In a conservative matrix form, the SWE including sewer source term read:

$$\partial_t \mathbf{U} + \partial_x \mathbf{F}(\mathbf{U}) + \partial_y \mathbf{G}(\mathbf{U}) = \mathbf{S}(\mathbf{U}) \tag{1}$$

In Equation 1, (x , y) are the spatial Cartesian coordinates and t is the time (SI units). **U** is the vector containing the flow variables, and **F(U)** and **G(U)** are the Cartesian components of the flux vectors. **S**(**U**) is the vector of source terms that, can be decomposed into $\mathbf{S} = \mathbf{S_s} + \mathbf{S_b} + \mathbf{S_f}$.

$$\mathbf{U} = \begin{pmatrix} h \\ hu \\ hv \end{pmatrix}, \ \mathbf{F} = \begin{pmatrix} hu \\ hu^2 + gh^2/2 \\ huv \end{pmatrix} \text{ and } \mathbf{G} = \begin{pmatrix} hv \\ huv \\ hv^2 + gh^2/2 \end{pmatrix} \tag{2}$$

$$\mathbf{S_b} = \begin{pmatrix} 0 \\ -gh\ \partial_x z \\ -gh\ \partial_y z \end{pmatrix}, \ \mathbf{S_f} = \begin{pmatrix} 0 \\ -C_f u\sqrt{u^2+v^2} \\ -C_f v\sqrt{u^2+v^2} \end{pmatrix} \text{ and } \mathbf{S_s} = \begin{pmatrix} V_S \\ -u_{bed}V_S \\ -v_{bed}V_S \end{pmatrix} \tag{3}$$

In Equations 2 and 3, g (m^2/s) is the constant gravitational acceleration; h (m) is the water depth, hu and hv (m^2/s) are the unit-width discharge expressed in terms of the velocity components u and v (m/s). $\mathbf{S_b}$ and $\mathbf{S_f}$ are, respectively, the topography and friction source terms involved in the momentum equations with $C_f = g\ n^2/h^{1/3}$ (n being the Manning roughness coefficient). $\mathbf{S_s}$ denotes a sewer flux term involved in the continuity equation in terms of vertical velocity V_s, which represents a *sewer* outflow into the floodplain; whereas u_{bed} and v_{bed} denote the local (i.e. non-depth averaged) horizontal velocities at the bed level, which are both zero at the solid surface and the vertical jet exit.

The system (Equation 1) is numerically solved over a 2D domain $[x_{min}; x_{max}] \times [y_{min}; y_{max}]$. The domain is discretised into computational $M \times N$ cells and a finite volume Godunov-type method is applied to explicitly solve the system over quadrilateral elements. A computation cell $I_i = [x_i - dx_i/2; x_i + dx_i/2] \times [y_i - dy_i/2; x_i + dy_i/2]$ is centred at (x_i , y_i) and has the dimension of $dx_i \times dy_i$. Over I_i, a local piecewise-constant solution $\mathbf{U_h}$ is sought and updated in time as:

$$\left(\mathbf{U_h}\right)_{I_i}^{n+1} = \left(\mathbf{U_h}\right)_{I_i}^{n} - \frac{dt}{dx_i}\left(\tilde{\mathbf{F}}_i^{E} - \tilde{\mathbf{F}}_i^{W}\right)^{n} - \frac{dt}{dy_i}\left(\tilde{\mathbf{G}}_i^{N} - \tilde{\mathbf{G}}_i^{S}\right)^{n} + \left(\mathbf{S}(\mathbf{U_h})\right)_{I_i}^{n} \quad (4)$$

In Equation 4, the superscript n denotes the present time status and dt the time step evaluated under the Courrant-Friedrich-Lewy (CFL) criterion with a CFL number of 0.5. The interface fluxes across eastern, western, northern and southern faces of cell I_i (i.e. $\tilde{\mathbf{F}}_i^{E}$, $\tilde{\mathbf{F}}_i^{W}$, $\tilde{\mathbf{G}}_i^{N}$ and $\tilde{\mathbf{G}}_i^{S}$) are obtained by the HLLC approximate Riemann solver (Toro et al. 1994). Bed, friction and sewer source terms are discretized in a local cell-centred manner (Wang et al. 2011).

NUMERICAL AND EXPERIMENTAL RESULTS

Experimental data

Using the physical model described in Section 2, ten steady flow experiments were conducted. Flow into the surface system Q_1 was kept constant in all cases (5.69 l/s), and all inflow measurements are within the stated 0.5% measurement error. The pipe discharge Q_3 was varied (increasingly) in order to produce the efflux $Q_e = Q_3 - Q_4$, which was positive in all case ranging between 2.1 *l/s* and 5.5 *l/s*). At the outflow of the floodplain, the discharge Q_2 was measured under free flow conditions (Figure 3 – left). Although the efflux Q_e(pipe) = $Q_3 - Q_4$ should equate $Q_2 - Q_1 = Q_e$(surface), from mass conservation principles, a difference in their value is noted. On average, the difference between Q_e(surface) and Q_e(pipe) is around 4.7%, which is consistent with the error related to the flow meters previously quantified. For each steady test, water levels are recorded at the six gauge points P0–P5 (Figure 3 – right). Points P2 and P3 are located along the x-centreline, respectively, at a distance of 90 mm upstream and downstream of the manhole. Whereas, points (P0, P1) and (P4, P5) are located along the y-direction, with P0 and P4 (respectively P1 and P5) located 75 mm (respectively 275 mm) far from the manhole.

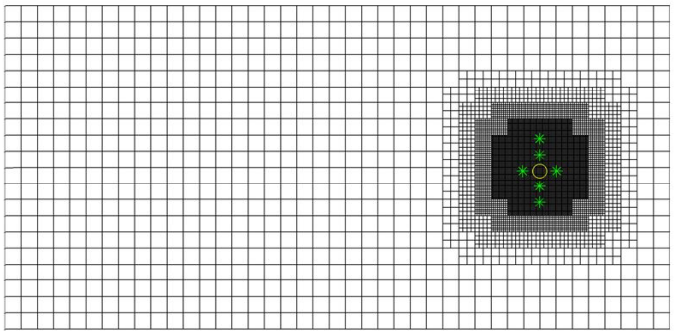

Figure 4. 2D quadrilateral mesh of the urban surface using a refined grid resolution of 0.0125 m^2 at the local zone of sewer-to-floodplain interaction, which is built upon a coarse mesh having a resolution of of 0.2 m^2

Numerical model setup

The numerical scheme (4) is applied on mesh consisting of quadrilateral elements. The initial number of quadrilaterals has been chosen to be 41 × 20 to generate a baseline (coarse) mesh with a spatial resolution of around 0.2m × 0.2m. This is the coarsest mesh possible in order to have, at least, one computational cell inside the circumference defined by the manhole diameter (i.e. 0.24 m). Such a

cell will be identified as manhole cell at which the $\mathbf{S_s}$ term in (3) in non-zero; more specifically, V_s will be involved as Q_e divided by the area of the manhole. To allow several manhole cells, local mesh refinement was applied to refine spatial resolution. Details on the mesh refinement method adopted are available in Liang (2012). As shows Figure 4, up to four levels of refinement are implemented around the local zone of sewer-to-floodplain interaction (resolution around 12.5mm × 12.5mm). The finest resolution also spanned the sampling points (P0-P5), to allow for sufficiently resolved modelling between manhole and the measurement points.

The discharge Q_e is fed into the numerical model through the involvement of V_s in the source term $\mathbf{S_s}$. For a single run, Q_e was defined from the different sources, i.e. Q_e(surface) and Q_e(pipe), in order to assess the sensitivity of numerical model relating to the uncertainty in flow measurements. For each Q_e, simulation is launched until convergence to a steady state is attained. A sensitivity analysis, relating to the experiments, suggested the use of a convergence threshold-error no bigger than 10^{-4} and no less than 10^{-6}. The initial discharge condition is taken to be the unit-width discharge relative to the inflow Q_1. Whereas, the initial depth condition is extracted from the outflow Q_2; namely, by either taking its normal depth or its critical depth. Nonetheless, the use of the normal depth is found to yield faster convergence; for efficiency, it was further adopted with a convergence threshold of 10^{-4} for all the simulations. At the eastern (upstream) boundary, the inflow Q_1 (in unit-width) is imposed and a (slip) numerical condition is used for the depth. At the southern and northern boundaries (lateral), wall numerical conditions are employed. At the western (downstream) boundary, two options are possible. The first is to use slip numerical boundary conditions in compliance with the (experimental) setup of a free outflow. The second option is motivated by the fact that the flow regime is identified subcritical at the outflow. Therefore, one physical outflow boundary condition maybe imposed (Kesserwani et al. 2008), which was here Q_2 (in unit-width) since no physical depth information was available.

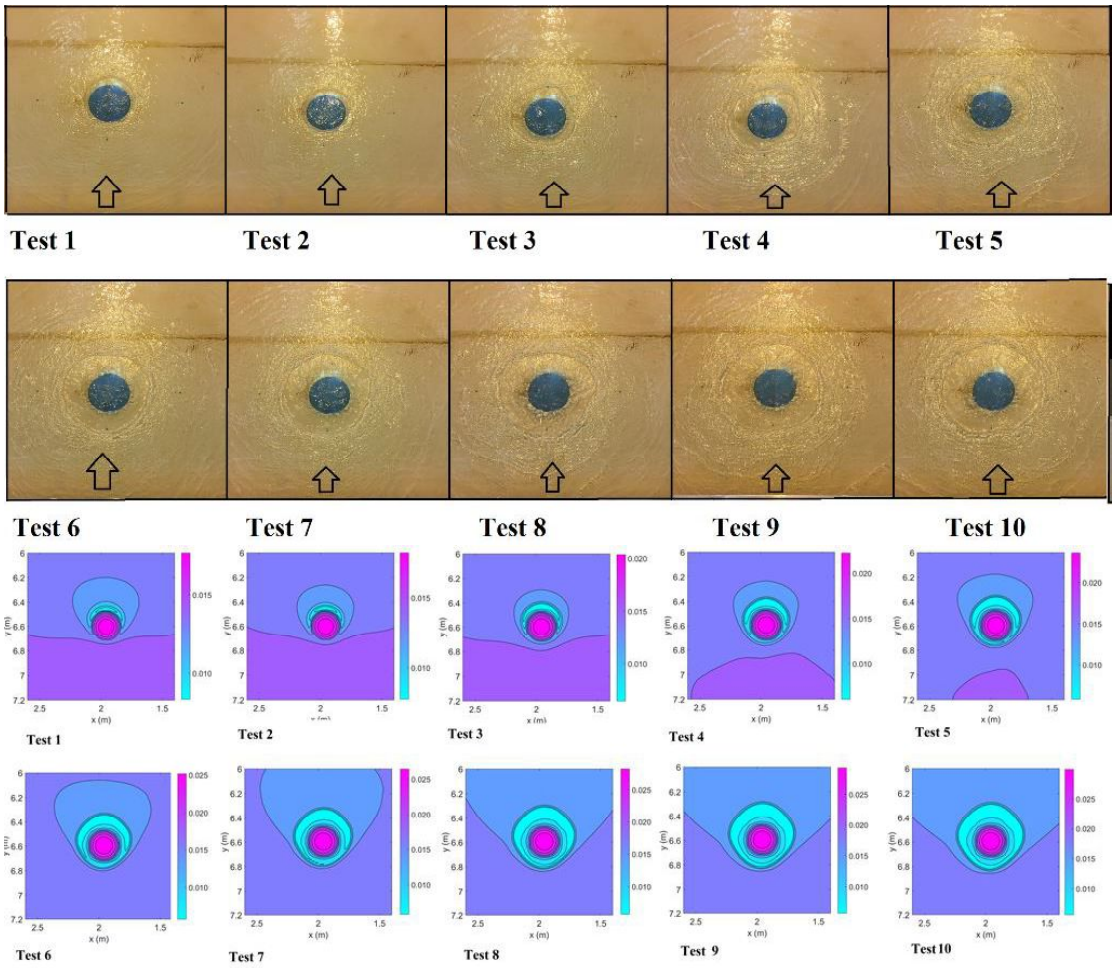

Figure 5. Water depth behaviour generated by the sewer-to-floodplain interaction with increasing efflux Q_e (i.e. Test 1-10): pictures taken during the experiments (upper part) and 2D simulation maps (lower part)

Comparison and discussions

In this section, experimental and numerical datasets are analysed. The process of sewer-to-floodplain flow interaction is first discussed in light of the 2D maps of the steady state simulations and snapshots of the flow patterns (taken during the experiments). Then, the predicted numerical and reported experimental depths at the gauges point P0-P5 are compared and discussed.

Flow patterns. Figure 5 displays zoom-in snapshots of the 2D depth maps (experimental and numerical) in the vicinity of the manhole area. Further analysis of the Froude number (numerical maps – not illustrated here) indicates a subcritical regime outside the area of sewer-to-floodplain interaction and rather one dimensional flow 1 m downstream of the manhole. In the manhole area, the vertical jet has constant velocity V_s. A bell-shaped 2D depth profile occurs, reaching its peak, along with null horizontal velocity. At the floodplain, the impact wave from the manhole leads to the formation of a circular water jump around the manhole. The magnitude of the water jump and the extent of the supercritical zone are observed to increase with increasing efflux discharge (Q_e). The impact of the steady inflow (Q_1) on the water jump is seen to be influential when $Q_e \leq 3.02$ *l/s* (Tests

1-3). In contrast, the span of the supercritical region and the front of the jump are clearly defined for higher efflux discharges.

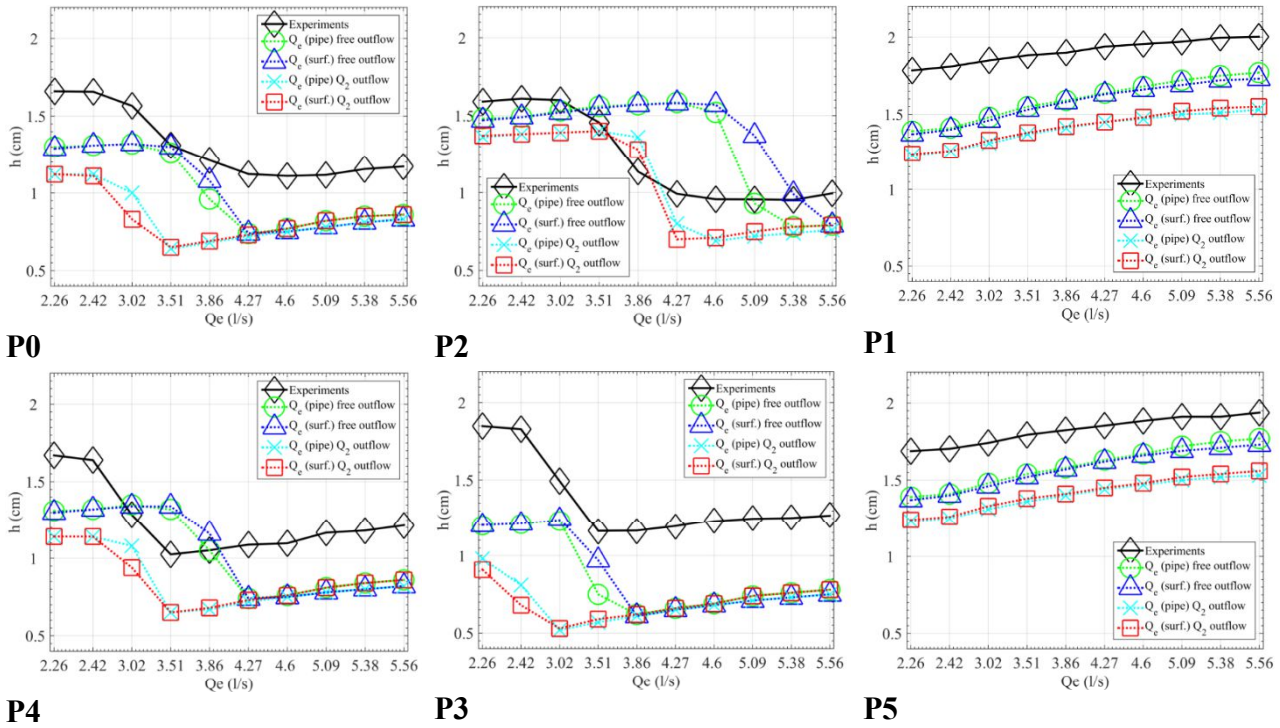

Figure 6. Steady state numerical and experimental depths compared at the sampling points around the manhole considering two different settings for (i) extracting Q_e and (ii) the outflow boundary condition

Simualtion vs. Experiments. The trends of the (experimental and numerical) water depths, produced at points P0-P5, are illustrated in Figure 6. At P0-P4, the behaviour of the experimental trends is seen to be quite similar, showing higher water levels for $Q_e \leq 3.02$ l/s and around 0.5 m lower water levels for $Q_e \geq 4.27$ l/s. This suggests that for the former Q_e, the water jump could not develop or did not have enough magnitude to produce supercritical flow closer to the manhole. For 3.02 l/s < Q_e < 4.27 l/s, gradual lowering in water levels is observed at P0 and P2, whereas the depths at P4 and P3 are more consistent with the lower depths predicted for $Q_e \geq 4.27$ l/s. Arguably, this is due to the fact that the flow at P0 and P2 is exposed to different wave reflections, since P0 is closer to the lateral boundary (than P4 – see Figure 1) and P2 is closer to the main inflow (where sewer overflow opposes the main flow). These may also be the reasons why the depth trends at P4 and P3 are slightly different (smoother) despite being at the same distance from P0 and P2, respectively, relative to the manhole. Slightly higher water levels at P3 are observed compared with those observed at P2; this is likely to be caused by the difference in ground levels at these points. Depth trends at points P1 and P5 are seen to increase with increasing Q_e, which is expected since these points were located at a farther distance from the manhole. However, the trend at P1 are somewhat higher, and this due to its closer positioning from the lateral wall (Figure 1).

In terms of numerical predictions, at all points, depth calculations are found to be relatively insensitive to the use of Q_e(pipe) or Q_e(surf.). In contrast, the effect of the downstream boundary is found to be much more influential on the numerical predictions, namely at the points situated closer to the manhole (P0, P4, P2 and P3). At P0 and P4, different depth predictions are noted, for Q_e < 4.27 l/s, in line with the two different type of boundary condition used. The predictions made by the

simulations using the *open boundary condition* are closer to the experimental data; they show an underestimating tendency apart from three results at point P4 where a slight overestimation is observed. The prediction delivered using the *imposed boundary condition* (Q_2– related), at P0 and P4, deviated more from the experiments; however, their overall trend is very consistent with the experimental data and does not show any overestimation. Quite similar behaviour is seen at P3 for Q_e < 3.86 l/s, which exclude any overestimation; most notably, here, the numerical predictions deviated further from the experiments. This discrepancy may be attributed to the depth-averaged assumption of the modelling approach adopted; because, at P3, the flow dynamics is highly 3D combining the flow cascading from around the manhole, entrained by the main inflow, with the upstream part of the water jump induced by the sewer overflow. At P2, the opposite is observed; the predictions relative to the *imposed boundary condition* provide better match to the experimental trend. The depths predicted by the use of the *open boundary condition* formed a different trend relative to the experimental data, albeit providing slightly better prediction for Q_e < 3.86 l/s. At point P1 and P5, the behaviour of the numerical calculations is entirely consistent with experimental predictions, showing slightly lower predictions in conjunction with the *imposed boundary condition*. Taken as a whole, the numerical and experimental predictions are generally in a very good agreement considering that (i) the discrepancy between is one average 5 mm, (ii) a depth-averaged numerical is adopted and (iii) no calibration measures were introduced to the numerical model.

SUMMARY AND CONCLUSIONS

This paper has explored the numerical and experimental modelling of the interaction between sewer overflow and floodplain flow. A physical model, linking a slightly inclined urban floodplain to a sewer system, was used to carry out measurements under steady state flow conditions. During an experiment, inflow and outflow discharges were measured at both the floodplain system and the sewer system. An experiment was conducted by fixing the floodplain inflow and varying the flow in the pipe so as to produce an increase in the sewer surcharge. Measurements of the inflows and outflows have defined Q_e to within an average difference of 4.7%, via mass conservation principles. Ten steady state experiments were conducted during which water levels at sampling points, surrounding the manhole, were measured.

A finite volume numerical model was tailored to produce alterative simulation results. The model has been based on the shock-capturing Godunov-type framework solving the 2D depth-averaged shallow water equations. The contribution of the sewer overflow (Q_e) has been directly treated as a source term component (under the full pipe assumption). Quadrilateral elements were used to generate the 2D mesh with coarsest (vertical and horizontal scale) resolution smaller than the manhole diameter. Four levels of mesh refinement were achieved spanning the location of the manhole and sampling points. Steady state simulations were achieved relative to each test, i.e. driven by the floodplain inflow (Q_1) and the sewer overflow (Q_e). These simulations were explored using entirely free outflow (numerical) boundary conditions and by imposing Q_2 as (physical) boundary condition. The numerical model was applied without any calibration measures.

The numerical results have been compared to the experiments in terms of snapshots of flood maps around the manhole, and by comparing the trends of the depth profiles at sampling points. The numerical and experimental flood maps reveal a consistent capturing of a circular hydraulic jump occurring as a result of the sewer overflow Q_e, and larger shock magnitude and supercritical zone. Detailed comparisons at the sampling points show very consistent agreement between the trend of the numerical and experimental water levels, more specifically at those point located downstream of

the circular jump (P1 and P5). At the point closer to the manhole (P0, P4, P2 and P3), some discrepancies are observed relating to the choice of the downstream boundary condition. Yet, taken as a whole, the numerical predictions are predominantly consistent with the experimental data. It can be therefore concluded that the proposed is numerical approach is able to favourably model sewer-to-floodplain interaction. As a perspective, experimental and numerical works are underway to validate the reverse interaction from the floodplain into the sewer system and investigate time varying conditions.

ACKNOWLEDGEMENT

The research has been supported by the UK Engineering and Physical Sciences Research Council (grants ID: EP/K040405/1).

REFERENCES

Borsche, R., Klar, A. (2014). Flooding in urban drainage systems: coupling hyperbolic conservation laws for sewer systems and surface flow. *Int. J. Numer. Meth. Fluids* 76(11), 789-810.

Wang, Y., Liang, Q., Kesserwani, G., Hall, J.W. (2011). A 2D shallow flow model for practical dam-break simulations. *J. Hydraulic Res.* 49(3), 307–316.

Toro, E.F., García-Navarro, P. (2007). Godunov-type methods for free-surface shallow flows: a review. *J. Hydraulic Res.* 45(6), 737–751.

Toro, E. F.; Spruce, M., Speares, W. (1994), Restoration of the contact surface in the HLL-Riemann solver. *Shock Waves* 4: 25–34,

Kesserwani G, Ghostine R, Vazquez J, Ghenaim A & Mosé R (2008). Application of a second order Runge-Kutta discontinuous Galerkin scheme for the shallow water equations with source terms. *Int. J. Numer. Meth. Fluids*, 56,805-821..

Liang Q. (2012) A simplified adaptive Cartesian grid system for solving the 2D shallow water equations. *Int. J. Numer. Meth. Fluids*; 69(2):442–458.

Leandro, J., Chen, A. S., Djordjevic, S., Savic, D. A. (2009). Comparison of 1D/2D coupled (sewer/surface) hydraulic models for urban flood simulation. *J. Hydraul. Eng.* 135(6), 495-504.

Mahdizadeh, H., Stansby, P., Rogers, B. (2011). On the approximation of local efflux/influx bed discharge in the shallow water equations based on a wave propagation algorithm. *Int. J. Numer. Meth. Fluids* 66 (10), 1295-1314.

Mahdizadeh, H., Stansby, P., Rogers, B. (2012). Flood wave modeling based on a two-dimensional modified wave propagation algorithm coupled to a full-pipe network solver. *J. Hydraul. Eng.* 138(3), 247–25

Rubinato, M. Shucksmith, J.; Saul, A. J., Shepherd, W. (2013) Comparison between InfoWorks hydraulic results and a physical model of an urban drainage system. *Wat. Sci. & Tech.* 68 (2), 372-379.

Seyoum, S., Vojinovic, Z., Price, R., Weesakul, S. (2012). Coupled 1D and noninertia 2D flood inundation model for simulation of urban flooding. *J. Hydraul. Eng.* 138(1), 23-34.

Valero, D., García-Bartual, R., Andrés-Doménech, I., Vallés, F. (2012). Testing a complex hydraulic design of a sewer transition with FLOW-3D. Comparison with a physical model (2012). Application note, FlowScience, Inc.

Rubinato, M. (2015) Physical Scale Modelling of Urban Flood Systems. Thesis (Ph.D.) - University of Sheffield, http://etheses.whiterose.ac.uk/9270/.